Comparative Density Functional Study of Associative and Dissociative Mechanisms in the Rhodium(I)-Catalyzed Olefin Hydroboration Reactions

Christoph Widauer,[†] Hansjörg Grützmacher,*[,†] and Tom Ziegler*[,‡]

Department of Inorganic Chemistry, ETH-Zentrum, Universitätsstrasse 6, CH-8092 Zürich, Switzerland, and Department of Chemistry, University of Calgary, 2500 University Drive NW, T2N 1N4 Calgary, Alberta, Canada

Received December 14, 1999

The $[RhCl(PH_3)_2]$-catalyzed hydroboration reaction $C_2H_4 + HBR_2 \rightarrow H_3CCH_2BR_2$ (R = OH, 2R = OCH=CHO) was investigated by means of density functional theory type calculations using the Amsterdam density functional (ADF) program. In the first step, the borane adduct $[RhCl(\eta^2\text{-}HBR_2)(PH_3)_2]$ (**1**) forms from $[RhCl(PH_3)_2]$ and the borane HBR_2. Subsequently, C_2H_4 adds to **1** to give either $[RhClH(BR_2)(C_2H_4)(PH_3)_2]$ (**2**) (*associative pathway* **I**) or $[RhCl(\eta^2\text{-}HBR_2)(C_2H_4)(PH_3)]$ (**23**) (*dissociative pathway* **II**). Further branching arises because on both pathways either boron migration (**I.B**, **II.B**) or hydride migration (**I.H**, **II.H**) may occur as initial product-forming steps. It is found that the associative mechanisms, **I.B** and **I.H**, have rather similar energy profiles and the formation of product complexes $[RhCl(H_3CCH_2BR_2)(PH_3)_2]$ (**9**, **15**) by reductive elimination requires overcoming the highest activation barriers (∼9 kcal mol^{-1}). Overall, the **I.H** pathway may be slightly favored over **I.B** for an associative mechanism. In contrast, for the dissociative mechanism migration and elimination reactions are kinetically strongly differentiated. On the **II.B** pathway, C−B bond formation is hindered by a high activation barrier (19.5 kcal mol^{-1}), while reductive C−H coupling furnishing the product complex $[RhCl(H_3CCH_2BR_2)(PH_3)]$ (**31**) has a low barrier (6.5 kcal mol^{-1}). On the **II.H** pathway the reverse is found: C−H formation has a low barrier (8.4 kcal mol^{-1}), while reductive C−B formation has a high barrier (15.8 kcal mol^{-1}). In summary, the **II.B** pathway may be slightly more favorable for a dissociative reaction. Since side products (i.e., vinyl boranes, alkanes) are formed on the **I.B** and **II.B** pathways, we suggest that rhodium-catalyzed hydroborations are driven into a dissociative **II.H** reaction channel which is easier to control kinetically by using bulky electron-withdrawing phosphines as ligands in the catalyst.

Introduction

The transition-metal-catalyzed olefin hydroboration reaction with catecholboranes HBcat (cat = 1,2-$O_2C_6H_4$) using the Wilkinson catalyst $[RhCl(PPh_3)_3]$ has become an important and well-established synthetic method.[1] The reaction was first reported by Männig and Nöth in 1985.[1a] They proposed a *dissociative* mechanism which involves oxidative addition of HBcat to the catalytically active metal fragment $[RhCl(PPh_3)_2]$, followed by ethylene addition with simultaneous dissociation of one PPh_3 group, migratory insertion of olefin into the Rh−H bond, and reductive C−B bond coupling. Evans, Fu, and Anderson[2] suggested a related and more detailed mechanism. According to this mechanism, results for deuterium labeling experiments of selected catalytic hydroboration reactions are rationalized by reversible olefin complexation and reversible hydride migration. On the basis of their experiments, Burgess et al.[3] proposed an alternative *associative* mechanism which involves boron migration followed by β-H elimination (dehydrogenative borylation) as a competitive process in catalytic hydroborations.

Hydroboration has also been studied by theoretical methods. Unfortunately, recent ab initio studies only considered one or the other pathway on different model systems.[4] Musaev et al. presented results for C_s symmetry restricted MP2 calculations for the associative mechanism of the model reaction $HB(OH)_2 + C_2H_4 \rightarrow H_3CCH_2B(OH)_2$ with $[RhCl(PH_3)_2]$ as the catalytically active complex.[4a] They found that the most favorable pathway involves oxidative H−B bond addition to $[RhCl(PH_3)_2]$, followed by addition of ethylene *trans* to chlorine, migratory ethylene insertion into the Rh−B bond, and subsequent reductive C−H bond coupling as the rate-determining step of the catalytic cycle. With

* To whom correspondence should be addressed. H.G.: Fax, +41 1 632 10 90; E-mail, gruetz@inorg.chem.ethz.ch. T.Z.: E-mail, ziegler@ucalgary.ca.
[†] ETH-Zentrum.
[‡] University of Calgary.

(1) (a) Männig, D.; Nöth, H. *Angew. Chem., Int. Ed. Engl.* **1985**, *24*, 878. (b) Burgess, K.; Ohlmeyer, M. J. *Chem. Rev.* **1991**, *91*, 1179. (c) Evans, D. A.; Fu, G. C.; Hoveyda, A. H. *J. Am. Chem. Soc.* **1992**, *114*, 6671.

(2) Evans, D. A.; Fu, G. C.; Anderson, B. A. *J. Am. Chem. Soc.* **1992**, *114*, 6679.

(3) Burgess, K.; Donk, W. A. v. d.; Westcott, S. A.; Marder, T. B.; Baker, R. T.; Calabrese, J. C. *J. Am. Chem. Soc.* **1992**, *114*, 9350.

(4) (a) Musaev, D. G.; Mebel, A. M.; Morokuma, K. *J. Am. Chem. Soc.* **1994**, *116*, 10693. (b) Dorigo, A. E.; Schleyer, P. v. R. *Angew. Chem., Int. Ed. Engl.* **1995**, *34*, 115.

10.1021/om9909946 CCC: $19.00
Publication on Web 04/28/2000

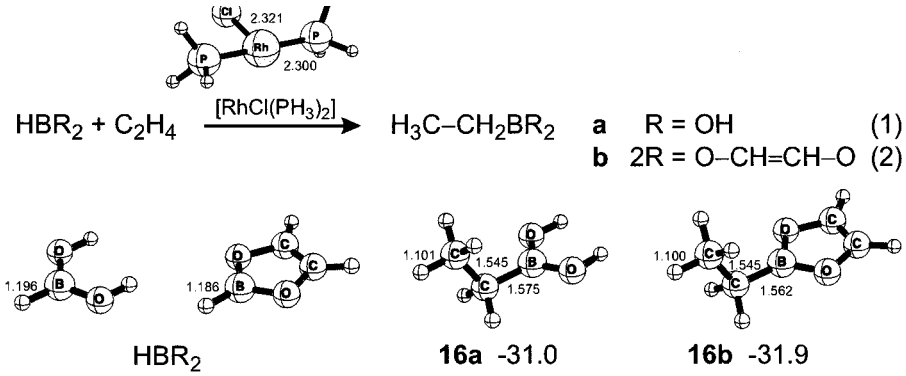

Figure 1. Model reactions (1) and (2) together with the optimized structures (selected bond lengths in Å) of the catalytically active complex $[RhCl(PH_3)_2]$ as well as the reactants HBR_2 and products $H_3CCH_2BR_2$ (R = OH, 2R = OCH=CHO). The energies (kcal mol^{-1}) are given relative to **0a,b**.

BH_3 instead of $HB(OH)_2$, Dorigo and Schleyer[4b] later reported results of their ab initio study of the dissociative mechanism, supporting the catalytic cycle originally presented by Männig and Nöth.[1a] These authors categorically excluded the possibility of an associative mechanism.

Here, we wish to report on the first detailed comparative study of the associative and dissociative mechanism of the model reactions $HBR_2 + C_2H_4 \rightarrow H_3CCH_2BR_2$ mediated by $[RhCl(PH_3)_2]$ (R = OH, 2R = OCH=CHO) by means of symmetry unrestricted density functional theory (DFT) type calculations.

Computational Details

All reported DFT calculations were performed by means of the Amsterdam density functional (ADF) program system developed by Baerends et al.[5] and vectorized by Ravenek.[6] The numerical integration scheme applied for the calculations was developed by te Velde et al.[7] The geometry optimization was based on the method of Versluis and Ziegler.[8] The electronic configurations of the molecular systems were described by an uncontracted triple-ζ STO basis set on the rhodium for 4s, 4p, 4d, 5s, and 5p.[9] A double-ζ STO basis set on the 1s shell for hydrogen and on the *n*s and *n*p valence shells for boron, carbon, phosphorus, and chlorine was used, augmented with a single $(n + 1)$d polarization function, except for hydrogen, where a 2p function was added. The inner shells on rhodium and all heteroatoms were treated within the frozen core approximation. A set of auxiliary[10] s, p, d, f, and g STO functions, centered on all nuclei, was used in order to fit the molecular density and present Coulomb and exchange potentials accurately in each SCF cycle. Energy differences were calculated by augmenting the local exchange-correlation potential by Vosko[11] et al. with Becke's[12] nonlocal exchange corrections and Perdew's[13] nonlocal correlation corrections. These corrections are known as the Becke88-Perdew86 exchange correlation functional.

All structures were optimized within C_1 symmetry including nonlocal corrections. No other constraints were applied if not mentioned otherwise. First-order (FO) scalar relativistic corrections[14] were added to the total energy for all optimized species. Transition states were obtained by coordinate driving. In this procedure all variables but the reaction coordinate (interatomic distance) were optimized and the reaction coordinate was stepwise decreased. The maximum of this linear transit served as the approximated transition state structure within the gradient accuracy of ±0.001 (au/Å).[15]

Results and Discussion

A. General Considerations. We studied the hydroboration reactions of C_2H_4 with the substrates $HB(OH)_2$ (eq 1) and $HBO_2(CH)_2$ (eq 2) involving the model Wilkinson catalyst $[RhCl(PH_3)_2]$, as depicted in Figure 1. The net reactions $HBR_2 + C_2H_4 \rightarrow H_3CCH_2BR_2$ were found to be exothermic by 31.0 kcal mol^{-1} for R = OH (eq 1) and 31.9 kcal mol^{-1} for 2R = OCH=CHO (eq 2), respectively. Structures related to reaction 1 will be referred to by numerals with the letter **a**, whereas numerals with the letter **b** refer to structures related to reaction 2. All energies for intermediates and transition states are relative to the total energy of $HBR_2 + C_2H_4 + [RhCl(PH_3)_2]$ (R = OH, 2R = OCH=CHO, denoted as **0a** and **0b**, respectively) given in kcal mol^{-1}.

We adapted the generally accepted catalytic cycle for the hydroboration reaction which involves initial addition of the borane to the catalytically active closed-shell d^8 complex $[RhCl(PH_3)_2]$,[16] followed by ethylene addition, further followed by migratory insertion of ethylene into the Rh−H or Rh−B bond and subsequent reductive elimination of the B−C or H−C bond, respectively (Scheme 1).

A closer view of the ethylene addition step $[RhCl(\eta^2\text{-}HBR_2)(PH_3)_2]$ (**1a**,**b**) + C_2H_4 is represented graphically in Scheme 2. After formation of the addition product **1a**,**b** various pathways can be accessed. Direct addition

(5) (a) Baerends, E. J.; Ellis, D. E.; Ros, P. *Chem. Phys.* **1973**, *2*, 41. (b) Baerends, E. J.; Ellis, D. E.; Ros, P. *Chem. Phys.* **1973**, *2*, 52.
(6) Ravenek, W. *Algorithms and Applications on Vector and Parallel Computers*; Elsevier: Amsterdam, The Netherlands, 1987.
(7) te Velde, G.; Baerends, E. J. *J. Comput. Chem.* **1992**, *99*, 84.
(8) Versluis, L.; Ziegler, T. *J. Chem. Phys.* **1988**, *88*, 322.
(9) (a) Snijders, J. G.; Baerends, E. J.; Vernoijs, P. *At. Nucl. Data Tables* **1982**, *26*, 483. (b) Vernoijs, P.; Snijders, J. G.; Baerends, E. J. Slater Type Basis Functions for the Whole Periodic System; Internal Report, Department of Theoretical Chemistry, Free University, Amsterdam, 1981.
(10) Krijn, J.; Bearends, E. J. Fit Functions in the HFS Method; Internal Report, Department of Theoretical Chemistry, Free University, Amsterdam, 1984.
(11) Vosko, S. H.; Wilk, L.; Nusair, M. *Can. J. Phys.* **1980**, *58*, 1200.
(12) Becke, A. *Phys. Rev.* **1988**, *38*, 3098.
(13) (a) Perdew, J. P.; Zunger, A. *Phys. Rev. B* **1986**, *33*, 8822. (b) Perdew, J. P.; Zunger, A. *Phys. Rev. B* **1981**, *23*, 5048.
(14) (a) Snijders, J. G.; Baerends, E. J. *Mol. Phys.* **1978**, *36*, 1789. (b) Snijders, J. G.; Baerends, E. J.; Ros, P. *Mol. Phys.* **1979**, *38*, 1909.
(15) For **TS-14a**, where the gradient could not be fixed to the gradient threshold, the geometry was located within an accuracy of ±0.0005 Å for the $B-C^2$ bond.
(16) Koga, N.; Morokuma, K. J. *J. Phys. Chem.* **1990**, *94*, 5454.

Scheme 1

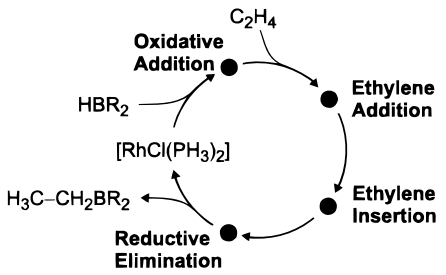

Scheme 2. Various Pathways for the Process of Ethylene Addition to 1a,b[a]

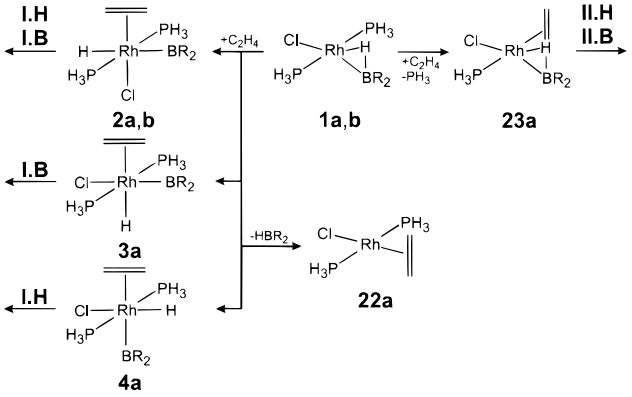

[a] Ethylene can directly attack from three different sides to the boron hydride complex **1**: *trans* to Cl (**2a**,**b**), *trans* to H (**3a**) and *trans* to B (**4a**), respectively. Complex **2a**,**b** is the key intermediate for the associative mechanism **I**, which can also be accessed via the corresponding isomers **3a** and **4a**. However, the parent borane HBR_2 easily eliminates from both **3a** and **4a**, leading to the ethylene complex **22a**. Ligand exchange between one PH_3 group and ethylene forms complex **23a**, which is the starting point for the dissociative mechanism **II**.

of ethylene generates complexes **2a**, **3a**, and **4a**. The key intermediate of the associative mechanism **I** is **2a**,**b**, in which ethylene binds *trans* to Cl. From complex **2a**,**b** pathways involve boron migration (**I.B**) or hydride migration (**I.H**). In principle, **I.B** as well as **I.H** can also proceed via the ethylene complexes **3a** and **4a**, where ethylene attacks *trans* to B or H, respectively. However, borane HBR_2 easily eliminates from **3a** and **4a** to form the ethylene complex $[RhCl(PH_3)_2(C_2H_4)]$ (**22a**). From **22a**, σ-bond metathesis can take place, involving direct insertion of the H−B bond into one Rh−C bond via a four-center transition state.[4a] This mechanism was proposed by Hartwig et al.[17] for the addition of HBcat to $CpRu(PPh_3)_2Me$.

Addition of ethylene to **1** with simultaneous dissociation of one PH_3 group leads to complex **23a**. This is the initial key intermediate for the dissociative mechanism **II** also involving pathways with both boron (**II.B**) and hydride migration (**II.H**).

In this paper, we present a comparative DFT study of the mechanisms **I** and **II**, for which we calculated the reaction profiles and energetics for the pathways involving boron migration (**I.B** and **II.B**) as well as hydride migration (**I.H** and **II.H**). On the basis of these data, controversial mechanistic models of the $[RhCl(PPh_3)_3]$-catalyzed hydroboration reaction will be discussed. In section B we present results obtained for the associative mechanism **I**, additionally considering β-H elimination from the product of boron migration in **I.B**. In section C, results for the dissociative mechanism are presented. In section D side reactions are discussed. In section E, we compare mechanisms **I** and **II** and section F contains the outlook.

Table 1. Relative Energies for Species Involved in the Associative Mechanism According to Eqs 1 and 2, Respectively[a]

	a, R = OH[b]			**b**, 2R = $O_2(CH)_2$	
0	0.0			0.0	
1 + C_2H_4	−43.9	(−7.2)	*−47.1*	−45.8	(−7.1)
2[c]	−35.5	(−13.0)	*−47.2*	−37.3	(−12.9)
3	−49.4	(−11.1)	*−67.1*		
4	−49.0	(−10.5)	*−71.0*		
TS-5				−36.9	(−12.2)
6	−53.7	(−8.4)	*−67.8*	−52.1	(−8.2)
7	−52.2	(−8.1)			
TS-8	−44.1	(−3.8)	*−45.4*		
9	−45.9	(−1.4)	*−52.6*		
TS-10	−35.2	(−11.4)			
11 + $[RhClH_2(PH_3)_2]$	−39.5	(−8.8)			
TS-12	−32.0	(−12.1)	*−40.7*	−34.5	(−12.3)
13	−59.1	(−8.1)	*−76.5*	−60.2	(−8.3)
TS-14	−50.2	(−4.6)	*−29.8*		
15	−56.2	(−3.1)			
16 + $[RhCl(PH_3)_2]$	−31.0	(0.1)	*−31.8*	−31.9	(0.1)
17	−50.0	(−7.8)			
18	−57.4	(−8.0)			
TS-19	−48.3	(−11.0)			
20	−48.4	(−7.8)			
TS-21	−45.3	(−9.1)			
22 + HBR_2	−45.6	(−5.3)	*−53.4*		

[a] All energies (kcal mol^{-1}) are relative to the total energy of $HBR_2 + C_2H_4 + [RhCl(PH_3)_2]$, denoted as **0a** and **0b**, respectively. Contributions of the relativistic corrections by first-order perturbation theory are given in parentheses. [b] Values given in italics are MP2 values taken from ref 4a. [c] **2a** is a restricted local minimum with $C^2-B = 2.616$ Å. **2b** is a free optimized local minima.

B. Associative Mechanism: Initial Steps. For all species involved in the associative mechanism **I** the energies are presented in Table 1. Selected bond lengths (Å) and angles (deg) for these compounds are given in Table 2.

Addition of $HB(OH)_2$ to $[RhCl(PH_3)_2]$ is exothermic by 43.9 kcal mol^{-1} to form the rhodium−borane complex **1a**. The geometry converged to a C_s symmetric square-planar complex, with the B−H bond forming one of the ligands. Some differences from the complex found by Musaev et al.[4a] are significant. In our calculations the B−H bond is much shorter (1.495 vs 1.995 Å) and, thus, the Rh−H bond becomes longer (1.641 vs 1.583 Å). This result suggests that the B−H bond in **1a** is still preserved to some extent.

In the next step ethylene can complex to **1a**, giving the products **2a**, **3a**, and **4a**, and the B−H bond is cleaved. The ethylene moiety takes a position either *trans* to the Cl, *trans* to H or *trans* to B (Figure 2).

In contrast to **3a** and **4a**, we were only able to optimize the ethylene complex **2a** with a *fixed* C^2-B distance (2.616 Å). However, as will be discussed later in this section, **2a** is comparable to the related derivative **2b**, which was optimized unconstrained (see Figure 5 and Tables 1 and 3). Thus, we assume that **2a** serves as a reliable model for an ethylene addition complex in the hydroboration reaction (1). The C−C bond distance in the three products of ethylene addition increases in

(17) Hartwig, J. F.; Bhandari, S.; Rablen, P. R. *J. Am. Chem. Soc.* **1994**, *116*, 1839.

Table 2. Selected Bond Lengths (Å) and Angles (deg) for the Optimized Geometries of the Generic Species Involved in the Associative Mechanism According to Eqs 1 and 2, Respectively[a]

	RhCl	RhH[b]	RhE[c]	BH	ClRhH	ClRhB	RhC[1]	RhC[2]	C[1]C[2]	C[1]H[d]	HRhC[1]	C[2]B	BRhC[2]
1a	2.395	1.641	2.072	1.495	167.8	146.5							
2a	2.459	1.674	2.181		85.3	87.0	2.182	2.182	1.417	2.400	75.7	2.630	74.1
3a	2.526	1.596	2.074	2.390	166.7	86.5	2.465	2.451	1.359	2.700	80.3		
4a	2.559	1.590	2.082	2.367	89.4	168.4	2.367	2.371	1.372			2.371	77.3
6a	2.513	1.552	*2.378*		101.2		2.123		1.539	2.594	88.4	1.573	
7a	2.441	1.558			139.5		2.198		1.530	2.226	72.8	1.585	
TS-8a	2.400	1.587			155.0		2.232		1.536	1.497	42.1	1.577	
9a	2.361	1.820	2.971		166.4	116.3	2.598		1.530	1.157	22.7	1.584	
TS-10a	2.480	1.642			89.1		2.151	2.249	1.435	2.766	92.6	1.563	
11a									1.342			1.557	
TS-12a	2.474	1.690	2.169		88.8	91.7	2.214	2.161	1.427	1.879	55.6	2.947	85.8
13a	2.453		2.018			124.2		2.130	1.520	1.107		2.597	77.5
TS-14a	2.396	*2.415*	2.064			139.8		2.239	1.526	1.010		1.890	68.8
15a	2.369	*1.802*	2.396			134.5		2.373	1.536	1.102		1.595	39.1
16a									1.545	1.101		1.575	
17a	2.445	1.559			144.7		2.121		1.524	2.19	71.2	1.576	
18a	2.460		2.012			121.4		2.135	1.521	1.106		2.647	79.3
TS-19a	2.550	1.636	2.090	1.750	94.0	148.4	2.269	2.255	1.395			3.000	87.2
20a	2.520	1.858	2.297	1.281	87.4	121.6	2.153	2.155	1.428			3.044	86.6
TS-21a	2.518	1.675	2.140	1.490	139.7	95.8	2.304	2.303	1.389	3.011	97.1		
22a	2.379						2.170	2.170	1.406				
1b	2.392	1.656	2.050	1.443	166.8	149.0							
2b	2.465	1.669	2.153		88.1	80.9	2.166	2.206	1.418	2.547	82.1	2.534	71.1
TS-5b	2.493	1.653	2.150		88.1	79.3	2.134	2.220	1.440	2.782	93.7	2.200	60.4
6b	2.500	1.545	*2.505*		102.2		2.128		1.542	2.531	85.5	1.559	
TS-12b	2.471	1.686	2.142		88.3	91.3	2.221	2.167	1.424	1.887	55.8	2.960	86.8
13b	2.445		2.000			130.0		2.131	1.523	1.108		2.555	76.3
16b									1.545	1.100		1.562	

[a] The ranges of some additional bond lengths and angles are given here: Rh−P, 2.320 ± 0.02 Å; B−O, 2.345 ± 0.005 Å; ClRhP, 87.0 ± 3.0°; OBO, 122.5 ± 2.5°. [b] RhH denotes the distance of Rh to the H originally bonded to B. The values in italics represent the distance between Rh and one of the C^2 hydrogens which undergo a β-agostic interaction in **15a**. [c] RhB distances are given in roman type. For **6a** and **6b**, respectively, the nearest Rh−O distances are given in italics. [d] C^1H denotes the distance of C^1 to the H originally bonded to B.

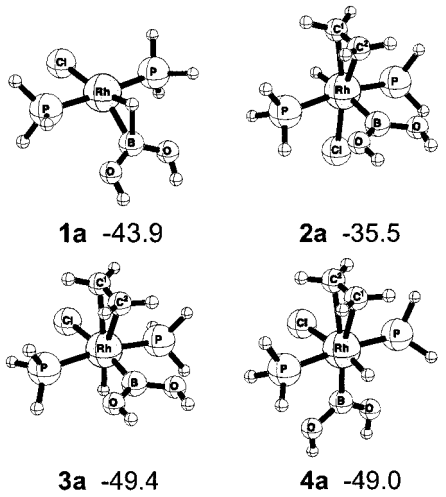

Figure 2. Optimized geometries of the borane complex **1a** together with the three isomers of associative ethylene addition **2a**, **3a**, and **4a**, respectively. The energies (kcal mol^{-1}) are given relative to **0a**.

the order 1.359 Å (**3a**) < 1.372 Å (**4a**) < 1.417 Å (**2a**). This can be rationalized by assuming that metal to ligand π back-bonding is weakest in the case where the boryl substituent is *trans* to the olefin and strongest when Cl is *trans* to the olefin (i.e., decreasing *trans* influence B ≈ H > Cl). In **2a** B and H are opposite to each other, thus mutually lengthening the Rh−H (1.674 Å) and Rh−B bonds (2.181 Å). In **3a** (Rh−H, 1.596 Å; Rh−B, 2.074 Å) and **4a** (Rh−H, 1.590 Å; Rh−B, 2.082 Å) the hydride and borane ligands take *cis* positions and the corresponding bonds are significantly shorter than in **2a**.

Table 3. Energy Decomposition Analysis of the Ethylene Addition Processes 1a → 2a and 1b → 2b[a]

	HRhB (deg)	DEF	INT	ΔE
1a → 2a	45.7 → 187.7	70.8 (11.5)	−56.6	14.2
	65.1 → 193.8	*73.6 (7.5)*	*−73.7*	*−0.1*
1b → 2b	44.2 → 191.0	69.8 (11.9)	−57.9	11.9

[a] Relative energies are given without relativistic energy corrections. DEF and INT are deformation and interaction energies, respectively. DEF(C_2H_4) is given in parentheses. ΔE is the binding energy DEF + INT. The values in italics are taken from ref 4a.

Musaev et al.[4a] calculated the ethylene addition process to be almost thermoneutral. Conversely, we found that the process **1a** + C_2H_4 → **2a** is clearly endothermic by 8.4 kcal mol^{-1} (14.2 kcal mol^{-1} without relativistic correction). Therefore, we reexamined the binding energy ΔE (Table 3) for **2a** according to eq 3.

$$\Delta E = \mathrm{DEF}(\mathbf{1a}) + \mathrm{DEF}(C_2H_4) + \mathrm{INT} \qquad (3)$$

DEF(**1a**) and DEF(C_2H_4) refer to the energies required for the reactant fragments **1a** and C_2H_4 to deform from their equilibrium geometries to the geometries observed in **2a**. INT is the interaction energy between the deformed fragments. Our results differ from those reported by Musaev et al., especially for INT, which is now calculated to be significantly smaller by 17.1 kcal mol^{-1}. Note that the inclusion of the relativistic correction (see Table 1) will diminish this energy difference to about 10 kcal mol^{-1}.

Boron Migration Preceding Reductive C−H Coupling (I.B). The associative pathway involving boron migration is depicted in Figure 3. All attempts to optimize **2a** led to direct conversion to the product of boron migration (**6a**), which is 18.2 kcal mol^{-1} more

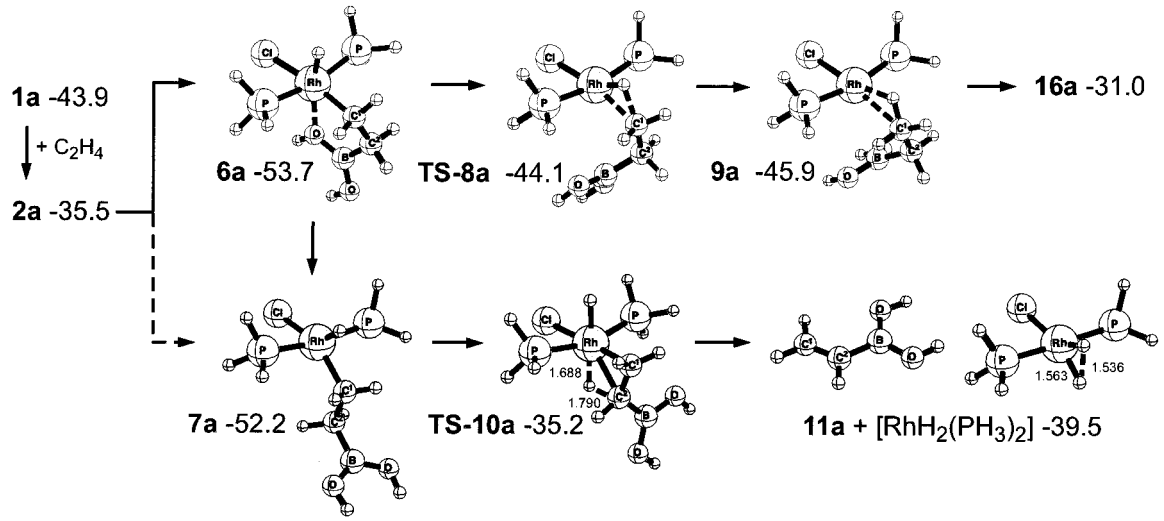

Figure 3. Reaction pathways for the associative mechanism **I.B** according to eq 1, which involves the formation of vinylborane **11a** and the hydride complex $[RhClH_2(PH_3)_2]$ via β-H elimination from **7a**. The energies (kcal mol^{-1}) are given relative to **0a**.

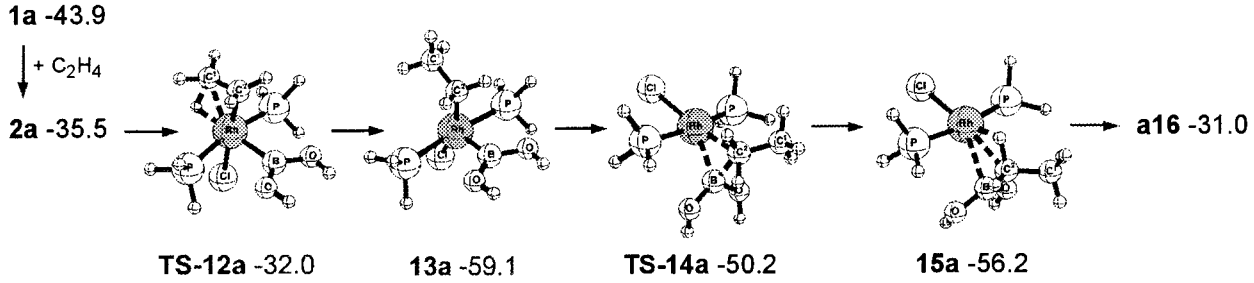

Figure 4. Reaction pathways for the associative mechanism **I.H** according to eq 1. The energies (kcal mol^{-1}) are given relative to **0a**.

stable than **2a**. The $B(OH)_2$ moiety in **6a** is rotated around the emerging $B-C^2$ bond (2.630 Å (**2a**) → 1.537 Å (**6a**)) to form a metallacycle in which one oxygen center interacts with the hexacoordinated rhodium center (Rh−O = 2.378 Å), which has a formal oxidation state of +3 (top of Figure 3). Subsequent reductive C^1-H bond formation leads to the product complex **9a** via the transition state **TS-8a** with a modest activation barrier of 9.6 kcal mol^{-1}, for which Musaev et al.[4a] determined a much higher barrier (22.4 kcal mol^{-1}). While the C^1-H bond is formed (2.594 Å (**6a**)→ 1.497 Å (**TS-8a**)→ 1.157 Å (**9a**)), the $B(OH)_2$ unit rotates around the $B-C^2$ bond and bends away from the metal center so that the Rh−O chelate bond is ruptured. The product complex **9a** is stabilized by the β-agostic $Rh-HC^1$ bond (1.820 Å). Finally, the hydroboration product $H_3CCH_2B(OH)_2$ (**16a**) dissociates from **9a**, a process which is endothermic by 14.9 kcal mol^{-1}. However, in solution this endothermicity would be reduced due to solvation of the generated metal fragment, which returns into the catalytic cycle.

Vinylboranes have been observed as side products in metal-catalyzed hydroborations, which may be formed by β-H elimination from intermediates such as **6a** (vide infra).[3] At first glance, β-H elimination from **6a** seems to be hindered due to the metallacycle formed by the chelate Rh−O bond. However, the Rh−O interaction in **6a** is weak and the corresponding isomer **7a** ($\tau(B-C^2-C^1-Rh) = 180°$) is only 1.5 kcal mol^{-1} higher in energy compared to **6a**. From **7a** β-H elimination is endothermic by 12.7 kcal mol^{-1}, leading to the hydride complex $[RhClH_2(PH_3)_2]$ and vinylborane $H_2C{=}CHB(OH)_2$ (**11a**) via **TS-10a** with a barrier of 17.0 kcal mol^{-1} (Figure 3). The hydride complex $[RhClH_2(PH_3)_2]$ is a model catalyst for *hydrogenation*, thus accounting for competitive H_2 addition to alkenes in transition-metal-catalyzed hydroborations (vide infra).

Hydride Migration Preceding Reductive B−C Coupling (I.H). The associative pathway involving hydride migration is depicted in Figure 4. Formation of complex **13a** is exothermic by 23.6 kcal mol^{-1} and proceeds via the early transition state **TS-12a** with a low barrier of 3.5 kcal mol^{-1}. In **TS-12a** the original geometry of the ethylene complex **2a** is only slightly distorted. In the course of the $H-C^1$ bond-forming process (2.400 Å (**2a**) → 1.879 Å (**TS-12a**) → 1.107 Å (**13a**)) the CH_3 group is rotated around the C^2-C^1 bond so that the ethyl moiety takes a staggered conformation with respect to the CH_2 group in **13a**. The reaction proceeds further by reductive elimination of the C^2-B bond to give the product complex **15a**, which is higher in energy by 6.0 kcal mol^{-1} compared to **13a**. The barrier for the endothermic C^2-B bond formation is calculated to be only 8.9 kcal mol^{-1}, in contrast to the very high barrier of 46.7 kcal mol^{-1} reported by Musaev et al.[4a] In the structure of the transition state **TS-14a** the ethyl group bridges the Rh−B bond, thus forming a 3c−4e bond within the three-membered RhC^2B cycle. In the product complex **15a** the Rh−B bond (2.396 Å) is almost completely ruptured and a β-agostic interaction is formed between one hydrogen of the C^2H_2 group and

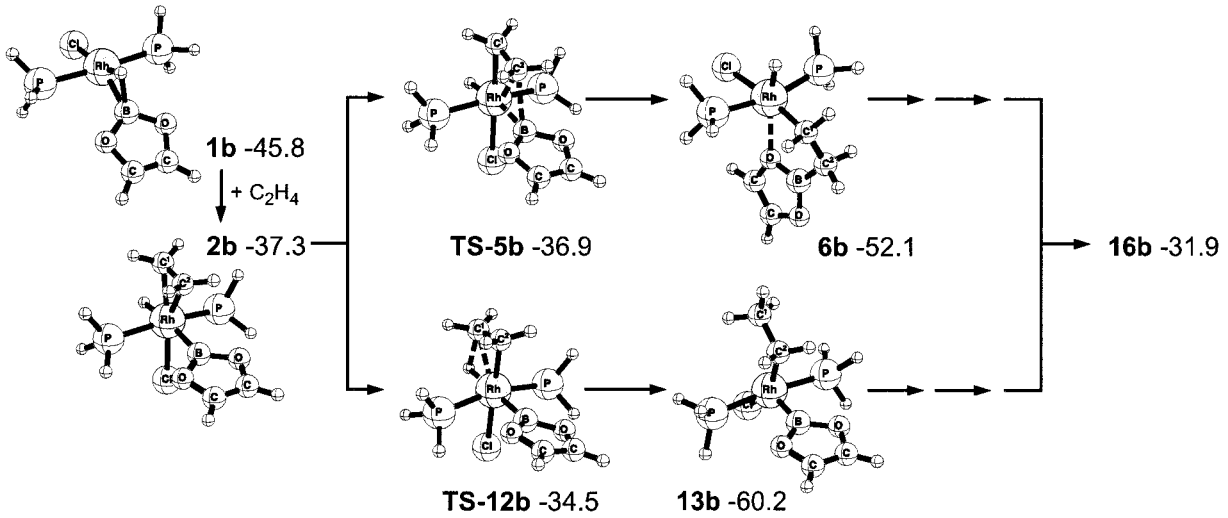

Figure 5. Reaction pathways for boron and hydride migration in the associative mechanism according to eq 2. The energies (kcal mol^{-1}) are given relative to **0b**.

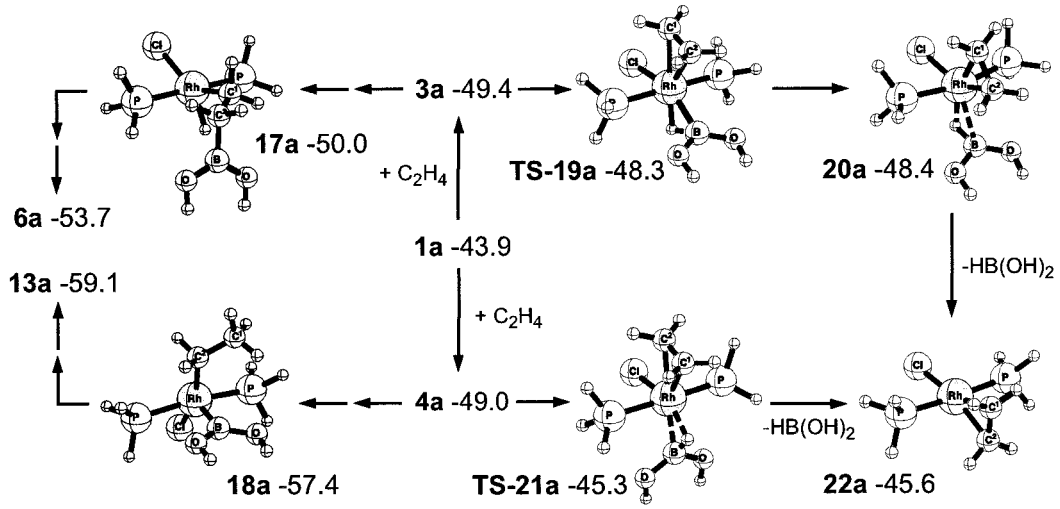

Figure 6. Accessibility of both pathways **I.B** and **I.H** from **3a** and **4a** via either **17a** or **18a**, respectively. Alternatively, reversible elimination of $HB(OH)_2$ leads to the ethylene complex **22a**. The energies (kcal mol^{-1}) are given relative to **0a**.

the metal center (Rh−HC² = 1.802 Å). Finally, dissociation of **16a** from the elimination product **15a** is endothermic by 22.0 kcal mol^{-1}. As already mentioned above, the required energy will be diminished by solvation of the catalyst.

Boron and Hydride Migration Reactions Starting from 2b. Because **2a** is not a fully optimized minimum, we calculated the first part of the associative mechanism using HBR_2, where 2R = OCH=CHO, according to the hydroboration reaction (2) as depicted in Figure 5.

The borane $HBO_2(CH)_2$ is even a more accurate model for HBcat (1,3,2-benzodioxaborole = catecholborane). In this case, we could optimize the product of ethylene addition **2b** without any constraints. The structure of **2b** corresponds well to **2a**. Migratory insertion of ethylene into the Rh−B bond is exothermic by 14.8 kcal mol^{-1}, leading to **6b** (top of Figure 5). We were able to locate its early transition state **TS-5b**, which is only 1.6 kcal mol^{-1} higher in energy than **2b**. For the formation of a heteroatom−carbon bond this barrier is surprisingly low. For the competitive migratory insertion of ethylene into the Rh−H bond the results are very similar to those obtained with $HB(OH)_2$: formation of **13b** is exothermic by 22.9 kcal mol^{-1}, proceeding via the transition state **TS-12b** with a barrier of 2.8 kcal mol^{-1} (bottom of Figure 5). The low barriers for both boron and hydride migration can be rationalized. First, as already discussed above for **2a**, the Rh−B and Rh−H bonds in **2b** are weakened mutually due to the strong *trans* influence of H and B, respectively. Second, borane and hydride are already very well disposed to interact with the π orbital of the incoming ethylene moiety.

Associative Pathways Starting from 3a and 4a. Ethylene addition to **1a** leading to **3a** and **4a** is exothermic by 5.5 and 5.1 kcal mol^{-1} compared to the endothermic formation (+8.4 kcal mol^{-1}) of the corresponding isomer **2a**. Thus, **3a** and **4a** are more stable by 13.9 and 13.5 kcal mol^{-1}, respectively, relative to **2a** due to the thermodynamically favored *cis* conformation of H and B. In principle, the products of boron migration and hydride migration, **6a** and **13a**, can be reached from **3a** and **4a** via the intermediates **17a** and **18a**, respectively (Figure 6).

We were not able to locate the corresponding transition states of the processes **3a** → **17a** and **4a** → **18a**. However, we assume from our calculations that their barriers must be significantly higher than those ob-

Table 4. Relative Energies for Species Involved in the Dissociative Mechanism According to Eq 1[a]

	a, R = OH[b]		
0	0.0		
1 + C_2H_4	−43.9	(−7.2)	*−76.4*
23 + PH_3	−37.6	(−6.4)	*−77.5*
TS-24 + PH_3	−18.4	(−7.8)	
25 + PH_3	−36.7	(−6.7)	*−60.2*[c]
26 + PH_3	−26.0	(−4.3)	
TS-27 + PH_3	−30.2	(−4.7)	
TS-28 + PH_3	−29.5	(−7.9)	*−73.4*
29 + PH_3	−29.4	(−6.0)	*−75.1*
TS-30 + PH_3	−13.6	(−3.5)	*−65.3*
31 + PH_3	−31.2	(−0.3)	*−81.1*
9	−45.9	(−1.4)	*−107.8*
16 + [RhCl(PH_3)$_2$]	−31.0	(0.1)	*−32.7*

[a] All energies (kcal mol^{-1}) are relative to the total energy of $HB(OH)_2$ + C_2H_4 + [RhCl(PH_3)$_2$] (**0a**). Contributions of the relativistic corrections by first-order perturbation theory are given in parentheses. [b] Values given in italics are taken from ref 4b relative to BH_3 + C_2H_4 + [RhCl(PH_3)$_2$] at the MP4(SDQ)/LANL1DZ(POL)//MP2/LANL1DZ level of theory. [c] For the **II.B** pathway starting with boron migration, Dorigo and Schleyer[4b] only considered the isomer {RhClH[$CH_2CH_2BH_2$](PH_3)} with phosphine in a position *trans* to the alkyl. In our calculations the isomer {RhClH[$CH_2CH_2B(OH)_2$](PH_3)} with phosphine in a position *trans* to the alkyl was found to be 16.1 kcal mol^{-1} higher in energy than **25a**.

served for the related processes **2a** → **6a** and **2a** → **13a** (see Figures 3 and 4). On the other hand, both complexes **3a** and **4a** easily eliminate $HB(OH)_2$, leading to the ethylene complex **22a**. These reactions are only slightly endothermic by 3.8 and 3.4 kcal mol^{-1}, respectively. Starting from **3a**, the process first reaches the intermediate **20a** via the transition state **TS-19a** with a barrier of only 1.1 kcal mol^{-1}. This reaction is almost thermoneutral, since intermediate **20a** is only 1.0 kcal mol^{-1} less stable than **3a**. Reductive elimination of $HB(OH)_2$ from **20a** leading to **22a** has no detectable barrier. The other pathway, reductive elimination of $HB(OH)_2$ from **4a**, leads directly to **22a** via **TS-21a** with a barrier of 3.7 kcal mol^{-1}.

Musaev et al.[4a] discussed mechanisms where HBR_2 adds directly to the ethylene complex **22a** to form C_s symmetric intermediates related to **17a** and **18a**, respectively. In these processes the B−C^2 and Rh−H (cf. **17a**) or H−C^1 and Rh−B bonds (cf. **18a**) are formed while the Rh−C^2 and B−H or Rh−C^1 and B−H bonds are broken simultaneously via a four-center transition state. However, we were not able to locate the corresponding transition states for these two processes. More likely, the linear transits show that readdition of HBR_2 to **22a** simply recovers **3a** and **4a**, respectively.

C. Dissociative Mechanism: Initial Steps. For all species involved in the dissociative mechanism **II**, the energies are presented in Table 4. Selected bond lengths (Å) and angles (deg) for these compounds are given in Table 5.

As shown in Scheme 1, addition of ethylene to **1a** together with simultaneous dissociation of one PH_3 group leads to complex **23a**. The process **2a** + C_2H_4 → **23a** + PH_3 is endothermic by 6.3 kcal mol^{-1}. The energy of **23a** + PH_3 relative to **0a** amounts to −37.6 kcal mol^{-1}, which is comparable in energy to the key intermediate for the associative mechanism, **2a** (−35.5 kcal mol^{-1}). In the complex **23a** the original geometry of the {RhCl(PH_3)[η^2-$HB(OH)_2$]} unit as found in **1a** remains almost unchanged. The ethylene moiety takes a position *trans* to the PH_3 group with Rh−C^1, Rh−C^2, and C^1−C^2 distances of 2.242, 2.266, and 1.378 Å, respectively.

Bearing only π acceptor (C_2H_4) or rather weakly σ donating ligands (Cl, PH_3, $HB(OH)_2$), the complex **23a** may be Lewis acidic. Therefore, we calculated the effect of solvent complexation on the ethylene addition process **1a** → **23a**, as shown in Scheme 3.

We chose THF as the most common solvent for [RhCl(PPh_3)$_3$]-mediated hydroborations. With THF the complex {RhClH[$B(OH)_2$](PH_3)(C_2H_4)(THF)} **S-23a** is formed, in which the B−H bond has now oxidatively added to the rhodium center, which augmented its formal oxidation state to +3. However, **S-23a** is only 3.9 kcal mol^{-1} lower in energy than separated **23a** + THF. This gain in enthalpy does not counterbalance the loss in entropy (∼10 kcal mol^{-1}) associated with THF complexation. Within the HSAB concept the low tendency of the "soft" Rh(+1) center in **23a** to coordinate to the "hard" donor THF is not surprising. Thus, we conclude that, at least for THF and other related "hard" donors, solvent coordination does not play an important role at this stage of the reaction. Thus, the dissociative mechanism indeed proceeds favorably via **23a**.

Boron Migration Preceding Reductive C−H Coupling (II.B). From **23a**, migratory insertion of ethylene into the Rh−B bond leads to the complex **25a** via transition state **TS-24a** (left side of Figure 7).

The step is slightly endothermic by 0.9 kcal mol^{-1}, with a high activation barrier of 19.2 kcal mol^{-1}. This finding may be rationalized as follows. First, the boronyl group has to rotate by 90° in order to bring its unoccupied p orbital into overlap with the filled π orbital of the ethylene moiety. Second, PH_3 and Cl exchange places in a piano-chair-like rotation in order to avoid that PH_3 and the emerging Rh−alkyl bond are opposite to each other, since both are strong *trans* directors and therefore avoid each other. In particular, by this thermodynamically highly favored rearrangement, 16.1 kcal mol^{-1} is gained with respect to the isomer of **25a**, in which the phosphine is in a position *trans* to the alkyl. In the course of the insertion of the boronyl group into the Rh−C^2 bond the B−C^2 bond emerges (3.083 Å (**23a**) → 1.875 Å (**TS-24a**) → 1.572 Å (**25a**)). In addition a chelating Rh−O bond (2.214 Å) is formed which stabilizes the electron-deficient metal(+3) center in complex **25a**. This intermediate is well disposed for the reductive C^1−H bond coupling via the transition state **TS-27a**, leading to the product complex **31a**, which is 5.5 kcal mol^{-1} higher in energy than **25a**. The moderate barrier for this step is 6.5 kcal mol^{-1}. During the C^1−H bond formation (2.167 Å (**25a**) → 1.570 Å (**TS-27a**) → 1.163 Å (**31a**)) the Rh−O interaction is maintained and the complex **31a** is further stabilized by an emerging β-agostic Rh−HC^1 bond (1.841 Å). Addition of PH_3 to **31a** is exothermic by 14.7 kcal mol^{-1} without an activation barrier, leading to complex **9a**.

Similar to the case for **6a**, dehydrogenative borylation from **25a** might take place. However, cleavage of the chelate Rh−O bond in **25a** to form **26a** is endothermic by 10.7 kcal mol^{-1}, whereas the formation of **7a** starting from **6a** costs only 1.5 kcal mol^{-1} in energy (see also

Table 5. Selected Bond Lengths (Å) and Angles (deg) for the Optimized Geometries of the Generic Species Involved in the Dissociative Mechanism of the Hydroboration Reaction 1[a]

	RhCl	RhP	ClRhP	RhH[b]	RhE[c]	ClRhH	ClRhB	RhC^1	RhC^2	C^{1}C^2	C^{1}H[d]	HRhC^1	C^{2}B	BRhC^2
23a[e]	2.386	2.322	83.9	1.651	2.110	166.1	150.2	2.242	2.266	1.378	2.632	83.6	3.083	89.5
TS-24a	2.450	2.311	87.8	1.584	2.147	170.9	120.2	2.067	2.181	1.461	2.569	88.4	1.875	51.2
25a	2.459	2.215	103.0	1.561	*2.203*	152.1		2.093		1.534	2.222	73.3	1.572	
26a[f]	2.385	2.187	96.8	1.554		140.7		2.070		1.513		73.0	1.591	
TS-27a	2.387	2.204	95.5	1.587	*2.196*	156.7		2.181		1.539	1.570	46.0	1.576	
TS-28a	2.402	2.352	87.5	1.645	2.010	174.2	99.7	2.235	2.145	1.427	1.535	43.4	3.084	95.8
29a	2.362	2.374	91.4	1.790	2.006	167.7	93.2	2.309	2.098	1.471	1.234	32.0	3.031	95.2
TS-30a	2.353	2.316	83.2	1.854	2.086	174.5	92.0	2.344	2.134	1.509	1.180	29.8	1.990	56.2
31a	2.332	2.195	92.1	1.841	*2.214*	162.5		2.445		1.538	1.163	27.1	1.579	

[a] For selected structural parameters of **1a** and **9a** see Table 2. [b] RhH denotes the distance of Rh to the H originally bonded to B. [c] RhB distances are given in Roman type. For **25a**, **TS-27a**, and **31a**, respectively, the nearest RhO distances are given in italics. [d] C^{1}H denotes the distance of C^1 to the H originally bonded to B. [e] The BH bond distance in **23a** is 1.434 Å. [f] The agostic Rh−HC^2 bond in **26a** is 2.212 Å.

Scheme 3. Ethylene Addition for the Dissociative Mechanism Involving Coordination of One Additional Polar Solvent Molecule of THF[a]

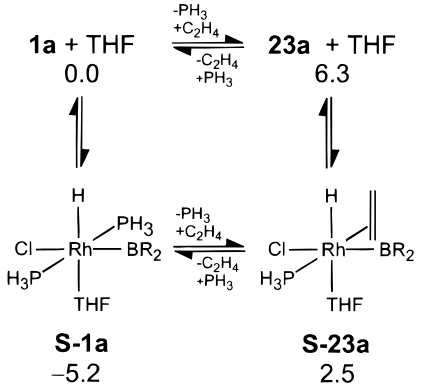

[a] The energies (kcal mol^{-1}) are given relative to **1a** + THF.

Chart 1). Thus, in the **II.B** pathway the formation of side products is much more hindered than in **I.B**.

Hydride Migration Preceding Reductive C−B Coupling (II.H). Hydride migration from **28a** is endothermic by 7.8 kcal mol^{-1}. The intermediate **29a** is reached via the transition state **TS-28a** (right-hand side of Figure 7). Inclusion of the relativistic perturbation correction causes **29a** to coincide with **TS-28a** within 0.1 kcal mol^{-1} in energy, so that both the kinetic and thermodynamic barriers for the process **23a** → **29a** becomes ∼8 kcal mol^{-1}. The coordination sphere in **TS-28a** may be best described as a square-planar pyramid in which the hydride (Rh−H = 1.645 Å), olefin (C^1═C^2), Cl, and P centers occupy basal positions while the boryl substituent is in an axial position. When the C^1−H bond is forming (2.632 Å (**23a**) → 1.535 Å (**TS-28a**) → 1.234 Å (**29a**)), the Rh−H bond is elongated and is changed into a β-agostic Rh−HC^1 interaction (1.790 Å) in the product **29a**. Subsequent reductive C^2−B coupling needs reorientation of the B(OH)$_2$ and C^{2}H$_2$ units, which leads to a substantial barrier of 15.8 kcal mol^{-1} for the C^2−B bond formation (3.031 Å (**29a**) → 1.990 Å (**TS-30a**) → 1.579 Å (**31a**)). This reductive bond coupling is slightly endothermic by 1.8 kcal mol^{-1}. Note that in **31a** the Rh(+1) center is stabilized by an intramolecular Rh−O interaction (2.214 Å) and the β-agostic Rh−HC^1 bond. Furthermore, there is a long Rh−C^1 contact (2.445 Å). PH$_3$ readdition to **31a** then leads to an exothermic reaction (14.7 kcal mol^{-1}) to **9a**, which is the common intermediate for the **I.B** pathway, in the associative reaction channel, and for both the **II.B** and **II.H** pathways, in the dissociative reaction channel. From **9** product release and catalyst recyclization takes place. The reaction profile calculated by Dorigo and Schleyer[4b] for the **II.H** pathway is shifted to much lower energies

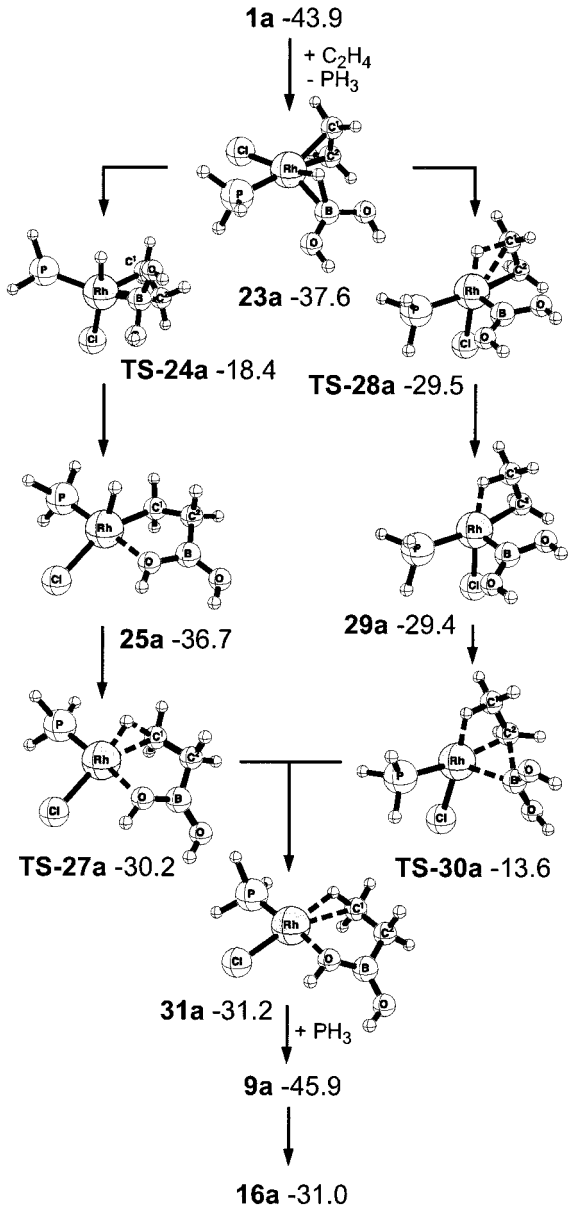

Figure 7. Reaction pathways for the dissociative pathways **II.B** and **II.H** according to eq 1. The energies (kcal mol^{-1}) are given relative to **0a**.

Scheme 4. Mechanistic Model According to Evans, Fu, and Anderson[2] To Rationalize α-Deuterium Incorporation with Reversible Hydride Migration

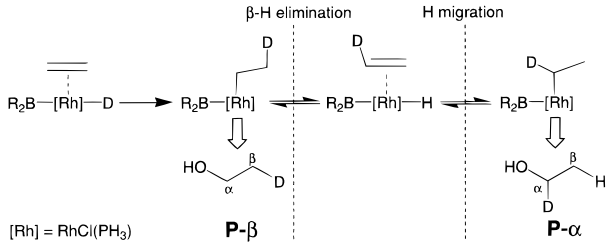

but is qualitatively similar to the one calculated herein (see Table 4 for comparison).

D. Side Reactions. Experimental observations, such as deuterium label incorporation on the hydroxyl (boronyl)-bearing carbon atom (e.g., eq 4), revealed unequivocally that competing processes must be operative in $[RhCl(PPh_3)_3]$-catalyzed hydroboration reactions.[2,3,18]

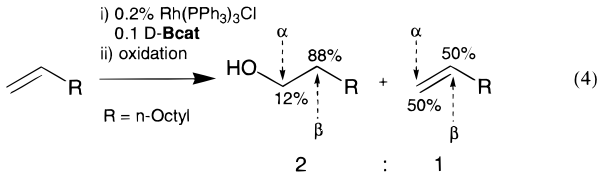

Evans, Fu, and Anderson[2] rationalized this observation with the original dissociative Männig-Nöth mechanism, i.e., oxidative HBcat addition → dissociative olefin complexation → hydride migration (**I.H**) → reductive C−B bond coupling. In addition, they assumed *reversible* hydride migration as well as *reversible* ethylene complexation in order to explain product and label distributions of various catalyzed hydroboration reactions (Scheme 4). In their mechanistic picture, boron migration preceding reductive C−H coupling (see **I.B** in Figure 3) is not considered.

Conversely, Burgess et al.[3] proposed an alternative associative pathway in which dehydrogenative borylation and *hydrogenation* (eq 5 and Scheme 5) compete with hydroboration.

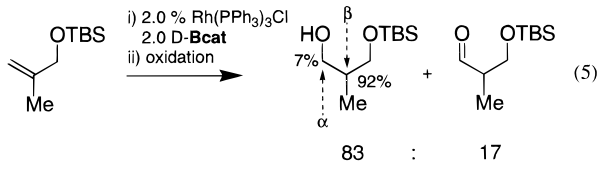

Hydride migration (**II.H**) is not excluded, but boron migration (**II.B**) followed by *β*-H elimination accounts for the formation of vinylboranes and the active hydrogenation catalyst $[RhCl(HD)(PPh_3)_2]$. This complex may promote HD addition to the vinylborane, which explains the α-D incorporation leading to the products **P-**α,*β*. Furthermore, HD addition to olefins may occur, which explains the formation of labeled alkanes (**SP-1** in Scheme 5).

(18) (a) Evans, D. A.; Fu, G. C. *J. Org. Chem.* **1990**, *55*, 2280. (b) Westcott, S. A.; Marder, T. B.; Baker, R. T. *Organometallics* **1993**, *12*, 975.

Scheme 5. Mechanistic Model According to Burgess et al.[3] To Rationalize α-Deuterium Incorporation and Formation of the Side Products SP-1 and SP-2, Respectively, with Boron Migration Followed by Subsequent *β*-H Elimination

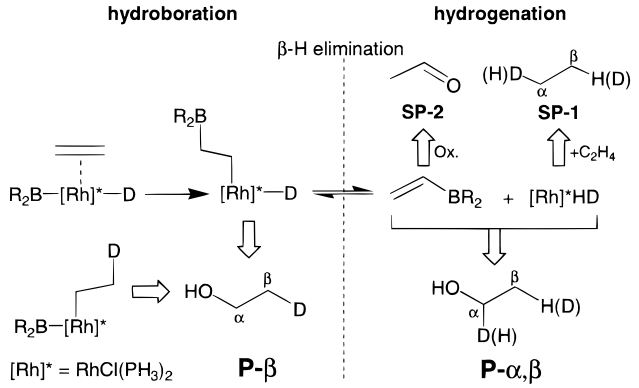

Dehydrogenative borylation explains also the observation of aldehydes (**SP-2** in Scheme 5) as side products (eq 5) in $[RhCl(PPh_3)_3]$-mediated hydroboration reactions. The precursors for their formation are vinylboranes, which have been detected and isolated in several metal-catalyzed olefin hydroborations.[3,18b,19] The formation of vinylboranes is reminiscent of the well-known formation of vinylsilanes in the course of catalyzed hydrosilylations.[19a,20]

E. Discussion: Associative (I.B and I.H) versus Dissociative (II.B and II.H) Reaction Pathways. In Scheme 6 the energy profiles for the two associative pathways **I.B** and **I.H** are compared with the two dissociative pathways **II.B** and **II.H**. For the associative mechanisms starting from **1a**,**b**, the energies shaded in gray obtained from calculations on eq 2 using the cyclic borane $HBO_2(CH)_2$ as hydroboration agent have been included. It is seen that both reactions are qualitatively very similar. Thus, although we have not considered the final steps of the hydroboration reaction (2) in detail, it can be assumed that they follow approximately the energy profile calculated for $HB(OH)_2$.

Most remarkably, both reaction channels, **I.B** and **I.H,** do not differ much in energy and both, **I.B** and **I.H**, are viable pathways for the formation of **P-***β* (Scheme 5) as the main hydroboration product in which H (D) binds to the *β*-carbon atom. After endothermic addition (∼8.5 kcal mol^{-1}) of ethylene to **1a** the hexacoordinated rhodium(+3) complexes $[RhClH(BR_2)(PH_3)_2(C_2H_4)]$ (**2a**, R = OH; **2b**, 2R = OCH═CHO) are obtained. From them both migratory insertion reactions, **I.B** under C−B formation and **I.H** under C−H formation, proceed via low-lying transition states (activation barriers <3.5 kcal mol^{-1}). The barriers for the **I.B** pathway are slightly lower.[21] However, the square-pyramidal rhodium(+3) complexes $\{RhCl(CH_2CH_3)[B(OR)_2](PH_3)_2\}$ (**13a**,**b**) formed on the **I.H** path are the most stable intermediates in the associative reaction channels, and thus **I.H** may well compete with **I.B**. Final reductive eliminations

(19) (a) Brown, J. M.; Lloyd-Jones, G. C. *Tetrahedron: Asymmetry* **1990**, *1*, 869. (b) Brown, J. M.; Lloyd, G. C. *J. Am. Chem. Soc.* **1994**, *116*, 866.

(20) Bergens, S. H.; Noheda, P.; Whelan, J.; Bosnich, B. *J. Am. Chem. Soc.* **1992**, *114*, 2128.

(21) Note that **2a** rearranges in our calculations to $\{RhClH[CH_2CH_2B(OH)_2](PH_3)_2\}$ (**6a**) even without an activation barrier.

Scheme 6. Potential Energy Surfaces for the Relevant Processes of the Associative Mechanism I and the Dissociative Mechanism II, Respectively[a]

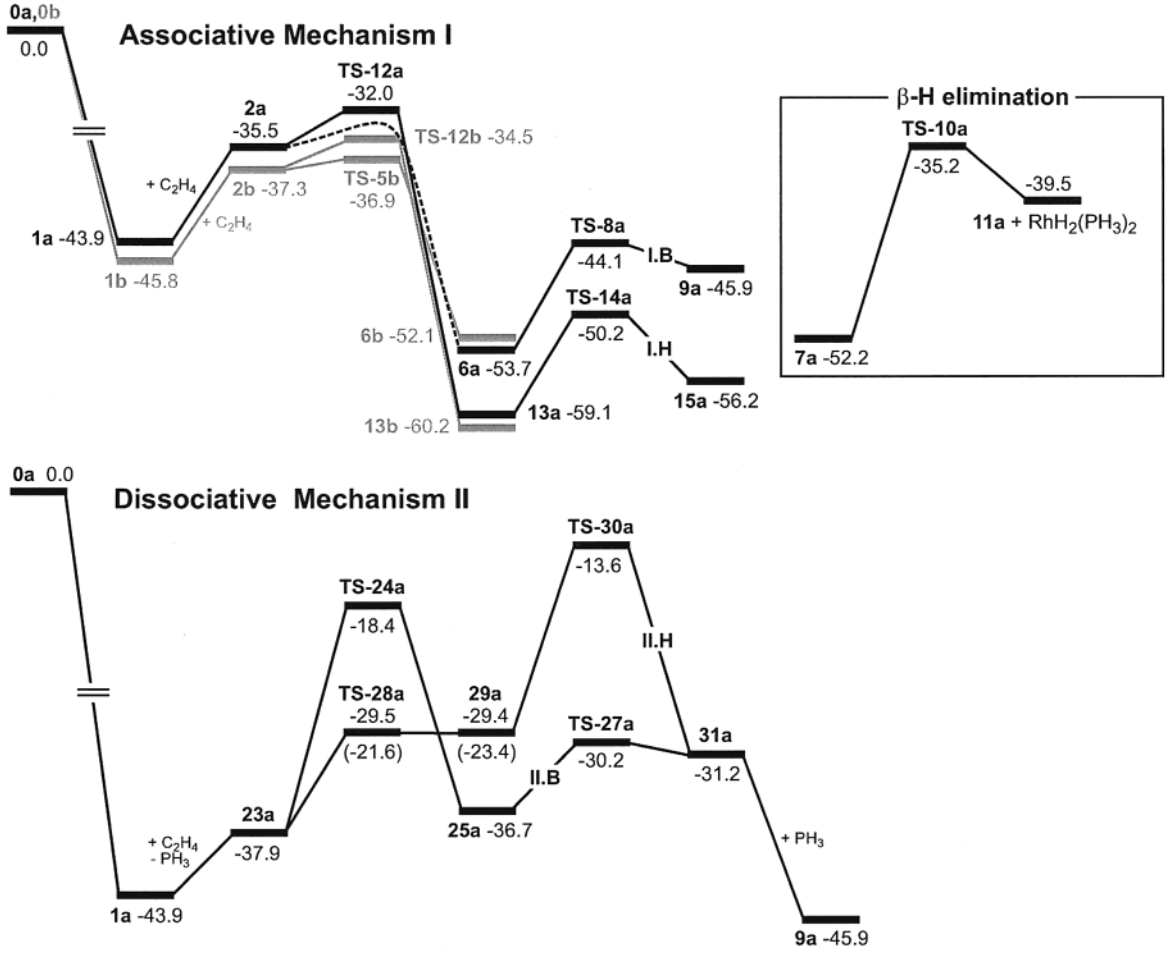

[a] For structures related to eq 1 the energies (kcal mol^{-1}) are given relative to **0a**, whereas for structures related to eq 2 the energies (kcal mol^{-1}) are given relative to **0b**. In the associative mechanism the reaction coordinates according to eq 2 are given in gray.

from **6a** (**6b**) in **I.B** and **13a** (**13b**) in **I.H** give the product complexes **9a** and **15a**, respectively, and require overcoming the highest activation barriers (~9 kcal mol^{-1}) on both pathways. In this case, the complex **15a** on the **I.H** path is kinetically and thermodynamically favored over **9a**. One may therefore assume that the migratory C−H insertion is slightly preferred for rhodium-catalyzed hydroborations following an associative mechanism; however, the **I.B** path involving initial C−B coupling to give **6a** competes efficiently with **I.H**. Note that the complex **6a** is also the key intermediate for the formation of side products [Rh]*H_2 ([Rh]* = [RhCl$(PH_3)_2$]) and $H_2C{=}CHB(OH)_2$ by β-H elimination as depicted in Scheme 6 (see also Figure 3). Although β-H elimination has a higher activation barrier (17.0 kcal mol^{-1} from **7a**) than reductive C−H coupling (9.6 kcal mol^{-1}), it may well be a feasible reaction in a real system. Therefore, it will be difficult to suppress the formation of side products (i.e., vinylboranes, alkanes) formed on the **I.B** path.

A comparison of the dissociative mechanisms **II.H** and **II.B** with the associative ones shows them to be thermodynamically disfavored; i.e., all intermediates **25a**, **29a**, and **31a** lie higher in energy than the corresponding intermediates **6a**,**b**, **13a**,**b**, **9a**, and **15a**. However, one has to take into account that for entropy reasons a dissociative reaction channel is favored over an associative one by about 10 kcal mol^{-1}, which actually diminishes the energy gap.[22] Most importantly, the pathways **II.B** and **II.H** are strongly *kinetically* differentiated with respect to the single reaction steps. On the **II.B** pathway, the migratory B−C insertion as initial product-forming step is hindered by a high activation barrier (19.5 kcal mol^{-1}). Subsequent reductive B−C coupling to give the alkylborane product complex {RhCl[H_3CH_2-$CB(OH)_2$](PH_3)} (**31a**) requires conquering a barrier of only 6.5 kcal mol^{-1}. On the other hand, migratory C−H insertion on the **II.H** pathway has a much lower barrier (8.4 kcal mol^{-1}), but subsequent reductive B−C coupling to give the product complex **31a** requires overcoming an activation barrier of 15.8 kcal mol^{-1} on the **II.H** path. Note also that the first intermediate {RhCl(CH_2CH_3)-$[B(OH)_2](PH_3)$} (**29a**) on the **II.H** path rearranges back by β-H elimination to the hydroborane complex {RhCl-[η^2-$HB(OH)_2$]$(PH_3)(C_2H_4)$} **23a**—which is thermodynamically favored—with no activation barrier (with inclusion of relativistic effects). This leads to a rapid installation of the preequilibrium **23a** ⇌ **29a**. In **II.B**, the intermediate {RhClH[$CH_2CH_2B(OH)_2$](PH_3)} (**25a**) formed by

(22) Remember that all energies given in Scheme 6 are relative with respect to [RhCl$(PH_3)_2$] + HBR_2 + C_2H_4 and entropy effects are not explicitly included.

initial boron migration is thermodynamically more stable than **29a** ($\Delta E = 7.3$ kcal mol^{-1}). Moreover, this complex will not react back to give **23a** but proceeds easily over **TS-27a** to yield the product complex **31a**. Therefore, according to our calculations, the **II.B** path may be favored in the dissociative reaction channel despite the high activation barrier for boron migration as the initial product-forming step. This is so because a rapid unfavorable preequilibrium and a subsequent high activation barrier hinders product formation on the **II.H** path. Side products can again form on the **II.B** branch from intermediate **25a**. Although we have not performed detailed calculations, one can assume that a conformation disposed to β-H elimination is accessible by Rh−O bond cleavage and rotation around the C^1-C^2 bond in **25a**. However, breaking the Rh−O bond in the unsaturated pentacoordinated Rh(+3) complex **25a** needs more energy (9.2 kcal mol^{-1}) than Rh−O bond cleavage in hexacoordinated **6a** encountered on the associative **I.B** path (see Chart 1). Therefore, the risk for side product formation should be lower in the dissociative reaction channels.

F. Outlook. We have applied pure quantum-mechanical methods (DFT) in a detailed study of the generic model reaction $C_2H_4 + HBR_2 \rightarrow H_3CCH_2BR_2$ (R = OH, 2R = OCH═CHO) mediated by the model Wilkinson's catalyst [$RhCl(PH_3)_3$]. The objective of this study has been to calculate the energy profile for various associative, i.e., ethylene addition without phosphine dissociation, and dissociative, i.e., ethylene addition with concomitant phosphine loss, pathways on an equal footing. Our results for the associative mechanism are in good agreement with propositions made by Burgess et al.[3] (Scheme 5). Since neither **I.B** nor **I.H** is thermodynamically or kinetically clearly favored, both are viable pathways for the formation of the main hydroboration product (**P-**β). Side products (vinylboranes, alkanes) stem from the **I.B** branch, and their formation will be difficult to avoid in an associative reaction. A different picture is seen for the dissociative reaction channels, where the risk for side product formation is lower. Moreover, migratory boron or hydride insertion as initial product-forming steps as well as C−H or C−B coupling on the **II.B** or **II.H** paths, respectively, have very different activation barriers. Although only **II.H** coincides with the mechanism proposed by Evans, Fu, and Anderson,[2] our calculations reveal that the alternative pathway **II.B** involving boron migration must be seriously considered and may be even preferred.

What ideas can we propose on the basis of this work which can be proven to be wrong or right by future experimental work? Given rhodium−phosphine complexes as catalysts for metal-promoted hydroborations, we suggest driving the reaction into a dissociative channel in order to suppress the formation of undesired side products. This may be done by employing sterically demanding electron-withdrawing ligands. Steric bulk should lead to a preference of the dissociative reaction mechanism. The electron-withdrawing properties will diminish the activation barrier for reductive C−H coupling on the **II.H** path, whereby the rhodium center changes its formal oxidation state from +3 (**29a**) to +1 (**31a**) (see Figure 7). On the other hand, the activation barrier for migratory boron insertion, i.e., **23a** → **25a**, where the formal oxidation state on the rhodium center is augmented from +1 to +3, will be raised, disfavoring the **II.B** path.

Chart 1

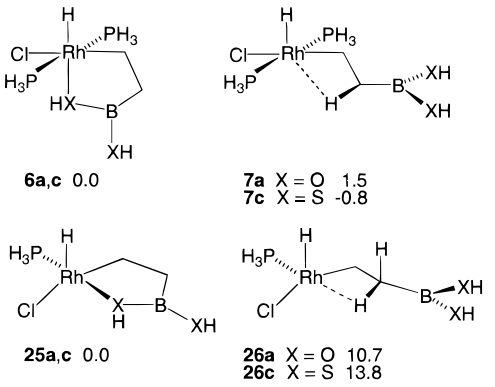

This latter path may become preferred when electron-donating bulky phosphines are used in connection with a borane containing donor centers, which bind more tightly to rhodium than oxygen (Chart 1). In this case, the dissociative mechanism **II.B** will be favored by augmenting the electron density on the metal, which raises the activation barrier for the reductive C−H coupling via **TS-30a**. In addition, boranes with soft donor atoms such as, for example, sulfur in thioboranes, $HB(SR)_2$, shall stabilize efficiently intermediates such as **25a** and **31a**. Thereby also the activation barriers leading to **25a** and **31a** are lowered. Furthermore, the transition state **TS-28a** of the C−B coupling profits directly from such a B-donor-atom−rhodium interaction.

Finally, we can predict that the formation of vinylboranes shall become favored in case small electron-donating phosphines bind to the metal center and a bulky alkyl- or arylborane, HBR_2, is used for hydroboration. Now the reaction may follow the associative **I.B** mechanism and β-H elimination may compete with reductive C−H coupling, since intermediates such as **6a** lack stabilization by donor atoms on the borane. On the other hand, acyclic intermediates such as **7a** (Figure 3) well prepared for β-H elimination are stabilized because the bulky borane residue positioned at the outer sphere of the molecule does not interfere with the other ligands. Actually, such a dehydrogenative borylation of olefins may be an interesting expansion of metal-catalyzed hydroborations, since vinylboranes are valuable intermediates for the preparation of carbonyl compounds.

Acknowledgment. The ETH Zürich and the Swiss National Science Foundation supported this work. This work has further been supported by the National Sciences and Engineering Research Council of Canada (NSERC). All calculations were carried out on the COBALT installations in Calgary. COBALT was bought by funds from a grant supplied by the Canadian Foundation of Innovation (CFI) with further support from the Intellectual Infrastructure Partnership Program (IIPP) from the province of Alberta and Nova Chemicals.

Supporting Information Available: Listings giving ZORA single-point energetics and *x*, *y*, *z* coordinates of all optimized species. This material is available free of charge via the Internet at http://pubs.acs.org.

OM9909946